Journal of Biomolecular Structure and Dynamics

ISSN: 0739-1102 (Print) 1538-0254 (Online) Journal homepage: http://www.tandfonline.com/loi/tbsd20

Molecular dynamics study of the dominant-negative E219K polymorphism in human prion protein

Samad Jahandideh, Mostafa Jamalan & Maryam Faridounnia

To cite this article: Samad Jahandideh, Mostafa Jamalan & Maryam Faridounnia (2015) Molecular dynamics study of the dominant-negative E219K polymorphism in human prion protein, Journal of Biomolecular Structure and Dynamics, 33:6, 1315-1325, DOI: 10.1080/07391102.2014.945486

To link to this article: http://dx.doi.org/10.1080/07391102.2014.945486

Accepted author version posted online: 16 Jul 2014.
Published online: 08 Aug 2014.

Journal of Biomolecular Structure and Dynamics, 2015
Vol. 33, No. 6, 1315–1325, http://dx.doi.org/10.1080/07391102.2014.945486

Molecular dynamics study of the dominant-negative E219K polymorphism in human prion protein

Samad Jahandideh[a]*, Mostafa Jamalan[b] and Maryam Faridounnia[c]

[a]*Program on Bioinformatics and Systems Biology, Sanford-Burnham Medical Research Institute, La Jolla, CA 92037, USA;* [b]*Department of Biochemistry, Ahvaz Jundishapur University of Medical Sciences, Ahvaz, Iran;* [c]*Bijvoet Center for Biomolecular Research, Utrecht University, Utrecht, The Netherlands*

Communicated by Ramaswamy H. Sarma

(*Received 15 January 2014; accepted 14 July 2014*)

Human prion diseases are associated with misfolding or aggregation of the Human Prion Protein (HuPrP). Missense mutations in the HuPrP gene, contribute to conversion of $HuPrP^{C}$ to $HuPrP^{Sc}$ and amyloid formation. Based on our previous comprehensive study, three missense mutations, from two different functional groups, i.e. disease-related mutations, and protective mutations, were selected and extensive molecular dynamics simulations were performed on these three mutants to compare their dynamics and conformations with those of the wildtype HuPrP. In addition to simulations of monomeric forms of mutants, in order to study the *dominant-negative effect* of protective mutation (E219K), 30-ns simulations were performed on E219K-wildtype and wildtype-wildtype dimeric forms. Our results indicate that, although after 30-ns simulations the global three-dimensional structure of models remain fairly intact, the disease-related mutations (V210I and Q212P) introduce local structural changes, i.e. close contact changes and secondary structure changes, in addition to global flexibility changes. Furthermore, our results support the loss of hydrophobic interaction due to the mutations in hydrophobic core that has been reported by previous NMR and computational studies. On the other hand, this protective mutation (E219K) results in helix elongation, and significant increases of overall flexibility of E219K mutant during 30-ns simulation. In conclusion, the simulations of dimeric forms suggest that the *dominant-negative effect* of this protective mutation (E219K) is due to the incompatible structures and dynamics of allelic variants during conversion process.

Keywords: Creutzfeldt–Jakob Disease (CJD); Gerstmann–Straussler–Scheinker disease (GSS); protective mutation; dominant-negative effect

1. Introduction

Transmissible spongiform encephalopathies, or prion diseases, are fatal neurodegenerative diseases caused by prions that occur in mammalian species (Prusiner, 1982). Prion diseases are including spongiform encephalopathy in cattle, scrapie in sheep, chronic wasting disease in deer and elk, and Creutzfeldt–Jakob disease (CJD) in humans (Van der Kamp & Daggett, 2011). In humans, sporadic CJD (sCJD) is the most common prion disease (Biljan et al., 2012).

The three-dimensional (3D) structures of prion proteins expressed by different species are very similar. The structure of Human Prion Protein (HuPrP) consists of a disordered N-terminal tail (residues 90–124) and a well-structured C-terminal region (residues 125–231). The globular core of wildtype (WT) HuPrP contains three α-helices (α_1: residues 144–155; α_2: residues172–192; α_3: residues 200–225), two short antiparallel β-sheets (β_1: residues 129–130; β_2: residues 162–163), and an intramolecular disulfide bridge linking helices α_2 and α_3 (Figure 1) (Zahn et al., 2000). The N-terminal tail of HuPrP is highly flexible and largely disordered compared to the C-terminal region, that is containing stable secondary structure elements (Figure 1) (Zahn et al., 2000).

Remained debated central dilemma of prion is the conversion of a properly folded prion protein to a scrapie form (PrP^{Sc}). This conversion includes a transition of α-helix structures into β-sheets; however, processes associated with the conversion of a properly folded prion protein into PrP^{Sc} are not clearly determined (Liemann & Glockshuber, 1998; Pan et al., 1993). In addition, decrease in pH and introduction of mutations are reported as promoting factors of the conversion into PrP^{Sc} (Van der Kamp & Daggett, 2011).

Up to now, several models have been proposed for PrP^{Sc}, but the tertiary structure of PrP^{Sc} has not been determined (Surewicz & Apostol, 2011). However, the main differences that discriminate PrP^{Sc} from well-folded prion protein are including partial protease resistance, amyloidogenicity, and the higher content of β-sheet (Biljan et al., 2012).

*Corresponding author. Email: sjahandideh@burnham.org

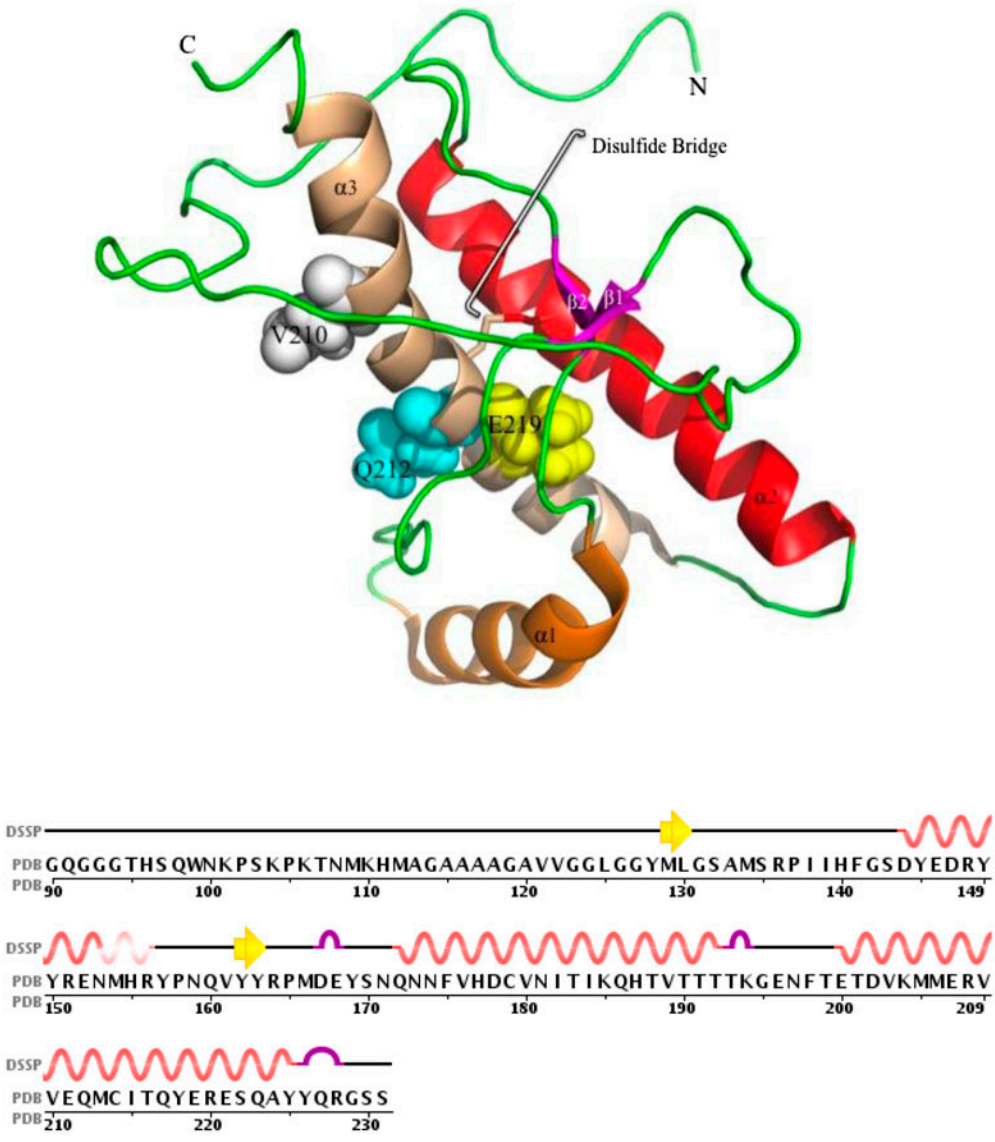

Figure 1. First, secondary, and tertiary structure of the HuPrP (2LSB PDB ID) containing three helices (α_1, α_2, and α_3), two short antiparallel β-sheets (β_1 and β_2), two turns, and an intramolecular disulfide bridge linking helices α_2 and α_3. Locations of three mutations of interest are shown.

Several supporting evidence in human shows the link between the mutations in HuPrP gene and prion diseases. From the three different types of mutations that exist, i.e. mutations resulting in a stop codon, insertion of additional octapeptide repeats in the N-terminus, and nonsynonymous mutations, only the third group is more studied theoretically and experimentally (Lukic et al., 2010; Panegyres et al., 2001; Polymenidou et al., 2011; Van der Kamp & Daggett, 2010).

E219K heterozygosis was found to protect against sCJD in Japanese population and also in Asian populations (Shibuya, Higuchi, Shin, Tateishi, & Kitamoto, 1998; Soldevila et al., 2003). In addition, the protective effect of E219K polymorphism, which also denoted as the *dominant-negative effect*, has been reported in several *in vivo* and *in vitro* experimental studies (Crozet et al., 2004; Geoghegan, Miller, Kwak, Harris, & Supattapone, 2009; Hizume et al., 2009; Kaneko et al., 1997; Lee, Yang, Perrier, & Baskakov, 2007).

Among all nonsynonymous point mutations, four of them including V180I, F198S, V203I, and V210I are located in the hydrophobic core. Also, T183A point mutation is related to the hydrophobic core mutants for its vicinity to the hydrophobic core and known to cause instability (Van der Kamp & Daggett, 2010). In a study by Van der Kamp and Daggett (2010), the effects of

these five mutations on the structure and dynamics of HuPrP were investigated using molecular dynamics simulations. Obtained results have shown a significant effect on the dynamics and stability of HuPrP, including the propensity to misfold, and increase in hydrophobic surface exposure (Van der Kamp & Daggett, 2010).

Because of a lack of experimentally solved mutant prion proteins, most of molecular dynamics (MD) studies on the effect of nonsynonymous mutations are done on *in silico* models. In this study, in order to provide more reliable results, we used experimentally characterized mutant- and WT-HuPrP structures that have been deposited into the Protein Data Bank (PDB IDs: 2LSB (WT), 2KUN (Q212P mutant), 2LEJ (V210I mutant), and 2LFT (E219K mutant)) (Biljan et al., 2012). We investigated the *dominant-negative effect* of E219K on its structure using built dimer heterozygous form of E219K-WT and compared to WT-WT dimer form. Monomeric and dimeric forms of the three mutants, mentioned above, were studied using MD simulation. In this regard, root-mean-square fluctuation (RMSF) values, root-mean-square deviation (RMSD) values, secondary structure changes, 3D structure changes, and close contacts were analyzed during the simulations. To summarize, obtained results support experimental results on the protective effect of E219K polymorphism and also explored novel approaches.

2. Methods

The MD simulations were performed using the Gromacs (version 4.5.5) software package (Van Der Spoel et al., 2005). The monomeric forms of WT and mutants that we used include these PDB IDs: 2LSB (WT), 2KUN (Q212P mutant), 2LEJ (V210I mutant), and 2LFT (E219K mutant) (Biljan et al., 2012). For dimeric forms, we used *in silico* mutagenesis on 1I4M (Knaus et al., 2001) to generate dimeric models for MD simulations. Before the production run of MD simulations, the protein structures were solvated with SPC model of water in a cubic cage. This cubic cage has a buffering distance of 10 Å between the edges of the box and the closest protein fragment. The number of water molecules in the cubic cage were approximately 15,000 for monomeric and 23,800 for dimeric models. To ensure that the total charge of the box was zero, the systems were neutralized by using sufficient Na^+ and Cl^- ions.

Next, all the systems were subjected to energy minimization through steepest descent method, followed by 100-ps of MD simulations in the canonical NVT ensemble. The minimized systems were equilibrated for a short 200-ps of MD runs with position restraints until the potential energy converged and stabilized at 300 K. Three separate MD simulations of 30-ns were performed for all equilibrated systems using GROMOS96 43a1 force field. The motion equations were investigated by using a leapfrog algorithm with a 2-fs time step and van der Waals forces were calculated with a 1.4 nm cutoff. For hydrogen bond analysis, only H-bonds with distance <0.35 nm between cooperated donor and acceptor heavy atoms and an angle of ≤ 30° were taken into account. In addition, stable salt bridges were extracted based on a distance cut-off value of 0.4 nm. The atomic coordinates of each model were saved every 50-ps for the analysis.

During the MD simulations, the root-means-square deviations of the *C*α-atoms (RMSD), RMSF, secondary structures changes, close contacts, and salt bridges were analyzed to consider conformational changes and stability of models during the MD simulations. The structural changes were visualized using MacPyMol (DeLano, 2002), and CMView packages (Vehlow et al., 2011).

3. Results and discussion

3.1. Structural stability and overall flexibility

For both monomeric and dimeric models, we ran 30-ns MD simulations. During the simulation of dimeric forms, the stability of complexes was considered through calculation of the number of H-bonds, free energy of binding, and electrostatistic (4r) energy. Figure 2 shows the average of changes in the number of H-bonds between monomers in dimeric models during 30-ns MD simulations. The number of H-bonds in E219K-WT is greater than WT-WT during MD 30-ns simulations and confirms stability of structures during simulations. On the other hand, the values for free energy of binding, and electrostatistic energy confirm the stability of dimeric models during 30-ns MD simulations (Table 1). K substitution for E at residue 219 is one of the main reasons for lower electrostatistic energy of E219K-WT complex rather than WT-WT complex.

The Cα-RMSD average values of the monomeric (WT and three mutants) and dimeric forms (E219K-WT and WT-WT) from the initial structures of HuPrP globular domains are shown in Figure 3. Figure 3(A) shows Cα-RMSD trends of native domain, protective mutation (E219K), and two disease-related mutations, i.e. V210I and Q212P, all in monomeric forms. After 2, 10, 15, and 20-ns, the average Cα-RMSD trends of WT-E219K, Q212P, V210I, and E219K monomer models comes into equilibrium with Cα-RMSD values of approximately 0.5, 1.5, 1.5, and 2 nm, respectively. This indicates that E219K has higher structural instability during MD simulation. A comparison of these values shows that there are three different trends and three different levels of instabilities existing, for three different categories of initial structure with a decreasing order of structural deviations with respect to the initial structures, i.e. protective mutation (E219K) > disease-related mutations (Q212P and V210I) > WT. Although for a long time it was

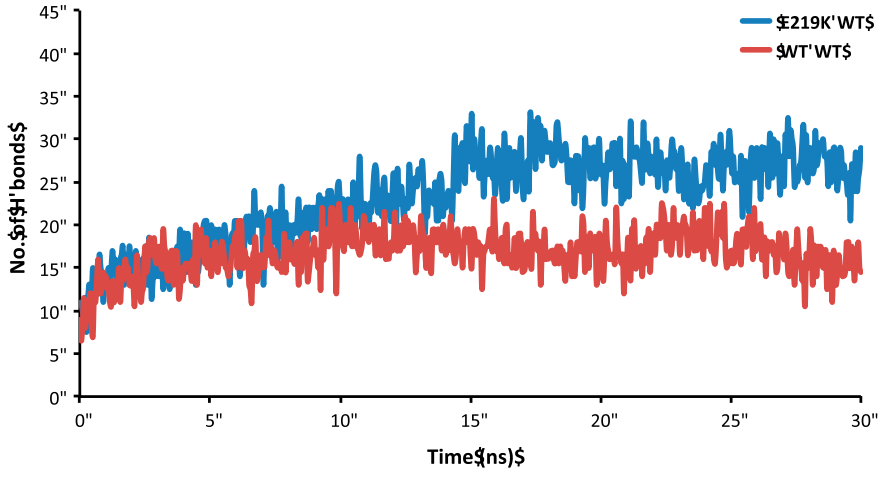

Figure 2. The average number of hydrogen bonds between protein domains in dimeric forms during 30-ns of MD simulations. Dimer of protective mutation and WT domain are shown in blue and dimer of two WT domains are shown in red.

Table 1. The average values of binding free energies and electrostatic energies for two docked dimeric forms after 30-ns of MD simulations.

Dimer	Free energy of binding	Electrostatic (4r) Energy (kcal/mol)
WT-WT HuPrP homodimer	−26.9	−42.8
E219K-WT HuPrP heterodimer	−46.6	−27.2

supposed that higher structural deviations in disease-related mutations could promote conformational rearrangements, our results are showing an exception. To tackle this raised question that how higher deviation is interpretable in protective ability of E219K mutation, we designed two dimeric models, i.e. WT-WT HuPrP homodimer vs. E219K-WT heterodimer to examine *dominant-negative effect* of E219K mutation and we ran 30-ns simulations on these models. As Figure 3(B) shows, the Cα-RMSD average values for WT domains in homodimeric models in a short time come into equilibrium with Cα-RMSD values of approximately 0.4 nm. This equilibrium persists until the end of 30-ns simulations. On the contrary, the Cα-RMSD average values of E219K domain in E219K-WT HuPrP heterodimer model comes into equilibrium after 10-ns with Cα-RMSD values of approximately 1.6 nm. This comparison of the stability of dimer forms is compatible with the results for the monomeric forms, which generally confirm the higher instability of protective mutations.

Figure 4 shows the Cα-RMSF average values for the monomeric models (WT and the three mutations mentioned earlier) and dimeric models (E219K-WT HuPrP heterodimer and WT-WT HuPrP homodimer) from the initial structures of globular domains of HuPrP. The Cα-RMSFs values for four monomeric model structures are shown in Figure 4(A). These results can explain the instability patterns of all monomeric model structures from the observed trends in Cα-RMSD average values (Figure 4). As Figure 4(A) illustrates, during the simulations, average values for two disease related mutants follow almost similar pattern of fluctuations, while WT domain and protective mutation follow patterns of fluctuations different from each other as well as disease-related mutations during the simulations. Although, significant fluctuations occur in disordered N-terminal tail (residues 90–124), the other flexible regions are located in loop regions with high values of structural flexibility that is in good agreement with the results of NMR studies (Biljan et al., 2012). Similarly as deviation results, protective mutation represent greater fluctuations in the dynamic behavior compared to the disease-related mutations and WT domain. It is understandable that the flexible segments are sequentially and spatially far from the mutation site. Thus, it may be concluded again that no direct contacts are responsible for these fluctuations in the protective mutation and disease-related mutations, and it could be due to the result of alterations in the global modulating forces. Furthermore, in order to explore the rationale of the *dominant-negative effect* of protective mutation, we averaged calculated Cα-RMSFs of E219K and WT domains in dimeric forms. Obtained results showed that E219K maintains high flexibility in dimeric form (Figure 4(B)). In order to come up with a

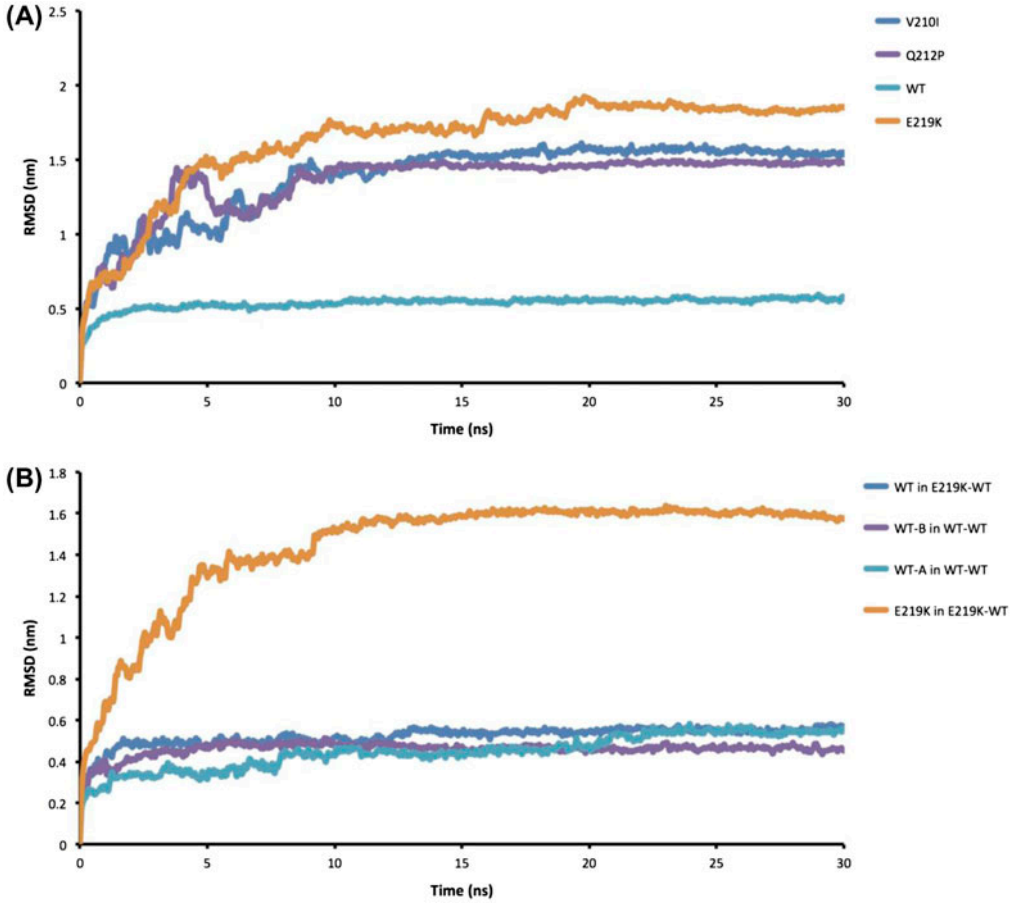

Figure 3. RMSDs average values of the Cα for structure models in monomeric and dimeric forms. (A) Average values of Cα-RMSDs for monomeric forms during 30-ns simulations. (B) Average values of Cα-RMSDs for dimeric forms during 30-ns simulations. WT-A and WT-B are WT domains in WT-WT homodimer model.

hypothesis about the role of flexibility in protective effect of E219K mutation, we extended our investigation to the consideration of secondary structure changes as well as close atomic contact changes during 30-ns MD simulations.

3.2. Secondary structure analysis

Two-dimensional plots of the secondary structure change as a function of the simulation time for monomeric and dimeric models that were generated. The obtained results on monomeric models are in good agreement with the previous MD studies on the disease-related mutations including our previous comprehensive MD study on all the nonsynonymous mutations of HuPrP (Chen, Van der Kamp, & Daggett, 2010; Guo, Ren, Ning, Liu, & Yao, 2012; Jahandideh & Zhi, 2014). Almost all mutant structures in the C-terminus of Helix 2 show the secondary structure shifts between helix and turn structures during the simulations, as well as shifts of the secondary structure between helix and turn structures in the C-terminus of Helix 3. In addition, as we have mentioned in this report and again explored the same results, E219K mutant structure is resistant to the *β*-sheet formation during simulation, whereas the formation of *β*-sheet for most of disease-related mutants is reported in literature. Therefore, the results in this study support previous studies. Furthermore, we studied the secondary structure changes during 30-ns MD simulation of dimeric forms, illustrated in Figure 5 as output of the first round of MD simulations. From this data, we have shown that an E219K mutant model is resistant to *β*-sheet formation even in dimeric form and diminishes the formation of *β*-sheet in its interacting WT partner and results in conversion of a few amino acids to 3_{10}-helix conformation in the vicinity of residue 110 in WT-HuPrP which is in complex with E219K mutant. The majority of the amino acid residues in N-terminal of E219K mutant in dimeric form are converted into coil conformation. In addition, during the simulations three helices in all monomers of dimeric models are stable.

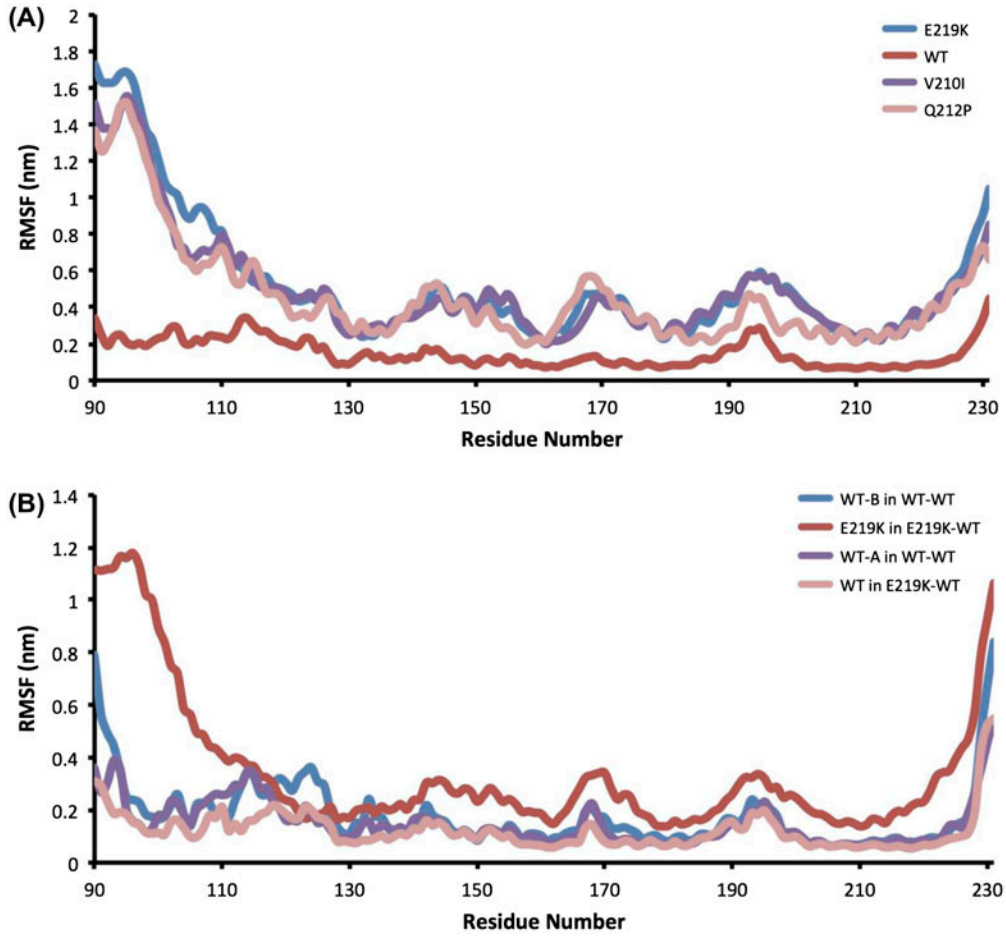

Figure 4. RMSFs average values of the Cα for structure models in monomeric and dimeric forms. (A) Average values of Cα-RMSFs for monomeric forms during 30-ns simulations. (B) Average values of Cα-RMSFs for dimeric forms during 30-ns simulations. WT-A and WT-B are wild type domains in WT-WT homodimer model.

3.3. Cα contact maps

Figure 6 shows the close contacts of WT HuPrP and four models after 30-ns MD simulations after the first round of simulations. In WT-HuPrP seven major close contact regions between different elements of globular domain of HuPrP include contacts between N-terminal tail and turn 1 (region 1), β_1 and β_2 (region 2), β_2 and α_2 (region 3), α_1 and α_3 (region 4), β_2 and α_3 (region 5), α_2 and α_3 (region 7) (Figure 6(A)).

In order to monitor changes of close contact regions for the structural models, we superimposed structural models with original WT each 5-ns during 30-ns simulations. For WT structure after 30-ns MD simulation, several contacts has been formed that many of them are related to the N-terminal disordered region. In total, at least eight contact regions appear after 30-ns MD simulation. In the N-terminal tail three contact regions appear (regions 1–3). The N-terminal tail residues 94–106 also make contacts to residues 164–167 (region 4). Two other contact regions with regard to residues 114–124 belong to the contacts with residues 158–163 including β_1 (region 5), and residues 182–185 in α_2 (region 6). The contacts in region 7 are increased to a large extent compared to WT (residues 131–136 and 209–221) including residues in β_1 and α_3. Region 8 consists of extensive contacts between the C-terminal of α_3 (residues 220–231) and the disordered N-terminal region (residues 104–114) while we observed very few contacts before simulation. In total, while contacts of β_2 to helices 2 and 3 decline after 30-ns MD simulations, N-terminal disordered tail and β_1 forms several contacts with different regions of the protein structure.

Results obtained for V210I are completely different. The first five residues of N-terminus form new contacts with residues 85–89 and 90–95 (regions 1 and 2). In region 3, a notably large contact region is formed between residues 105–115 and 116–128 and the contact network suggests formation of beta-sheets. The distances between the side-chains and backbones at this region are in many cases between 3 and 5 Angstrom. The residues

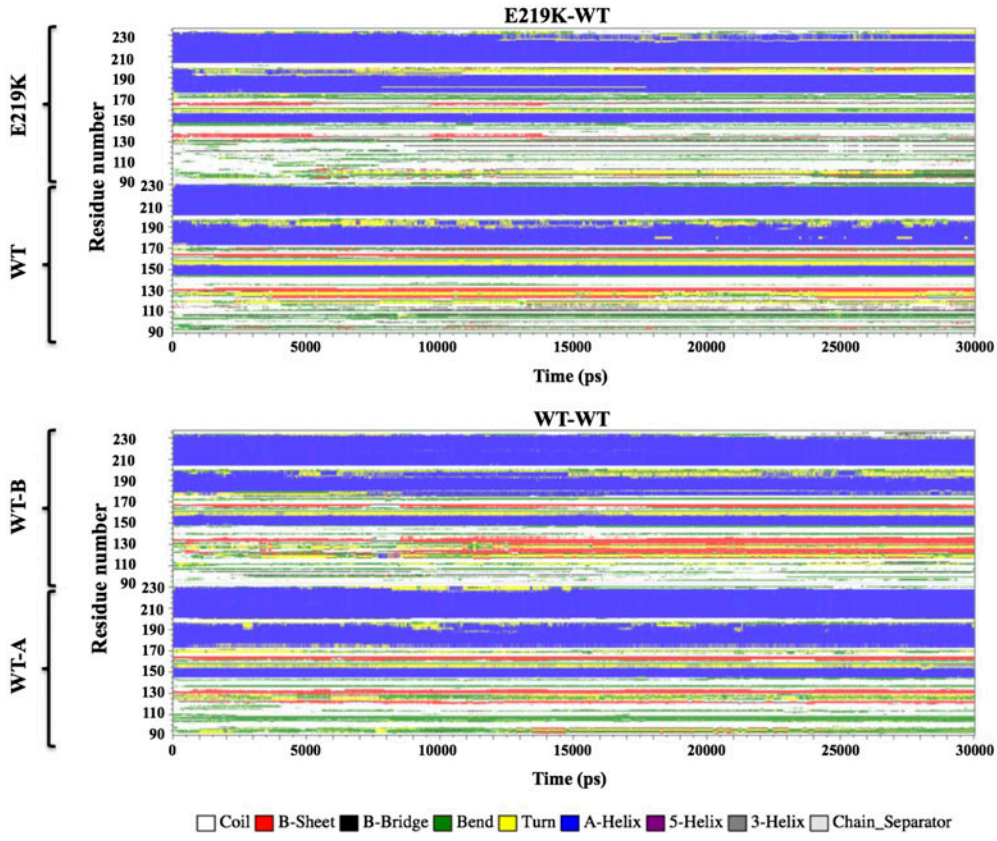

Figure 5. The secondary structure as a function of the simulation time for two dimeric model structures during the first round. Upper panel, and lower panel indicate secondary structure for the E219K-WT, and WT-WT dimers, respectively.

in region 116–128 also make some few contacts to residues 164–169 (region 4) and 182–186 (region 10). While contacts between N-terminal residues 94–100 and 169–172 (region 9) in E219K model are missing, it seems the contact network has relocated to the end of α_2 of HuPrP and the turn region, i.e. residues 191–198 (region 6). Similar changes are seen for regions 5 and 11. Also, some reorientations occur at the mutation site (region 8) and while some contacts are omitted some new contacts are formed between α_3 and the extended region. Interestingly, while the helicity is reduced in α_2 (residues 171–179), these residues make extensive contacts to residues at the C-terminal region at the end of α_3 with residues 122–131. Also parts of α_2 and α_3 (residues 91–105) form new contacts with residues 155–156 (region 7).

After 30-ns MD simulations of Q212P model, residues 90–96 in the N-terminal disordered tail make a network of contacts resulting in four new contacts regions (regions 1–4). Region 4 (residue 103–106) can also form contacts to residues 98–102 and present reorientations with regard to residues 165–172 (region 7). Furthermore, residues overlapping with region 4 (105–109) have contacts to residues 111–113 (region 5), while they lose their contacts to residues 219–223 (region 10). Within region 6, several local contacts are formed. In addition, we observe that residues 119–126 have contacts to α_2 residues (regions 9). Compared to the original WT structure, residues 127–136 including β_1 strand have more contacts to residues 157–166 (region 8) including β_2. Three more differences between Q212P model and original WT structure consist of residues 165–174 losing contacts to residues 175–179 probably due to α_2 shortening (region 12), while the N-terminal residues of α_2 helix are forming new connections with residues 214–233 at the C-terminal of α_3 helix and the C-terminal helix (region 13). To summarize, Q212P mutation results in extensive contacts between the N-terminal tail residues (regions 1–6), N-terminal tail and α_2 (regions 9 and 11), and reorientation of contacts between α_2 and α_3.

About the case of E219K model, after 30-ns MD simulations, N-terminal disordered tail residues 96–100 form new contacts to residues 90–96 (region 1) and residues 121–127 (region 3), while they lose contacts to residues 169–172 (region 5) compared to original WT structure. Instead we observe helix formation for residues 169–172 (regions 6); another contact region is formed in disordered tail between residues 101–105 and

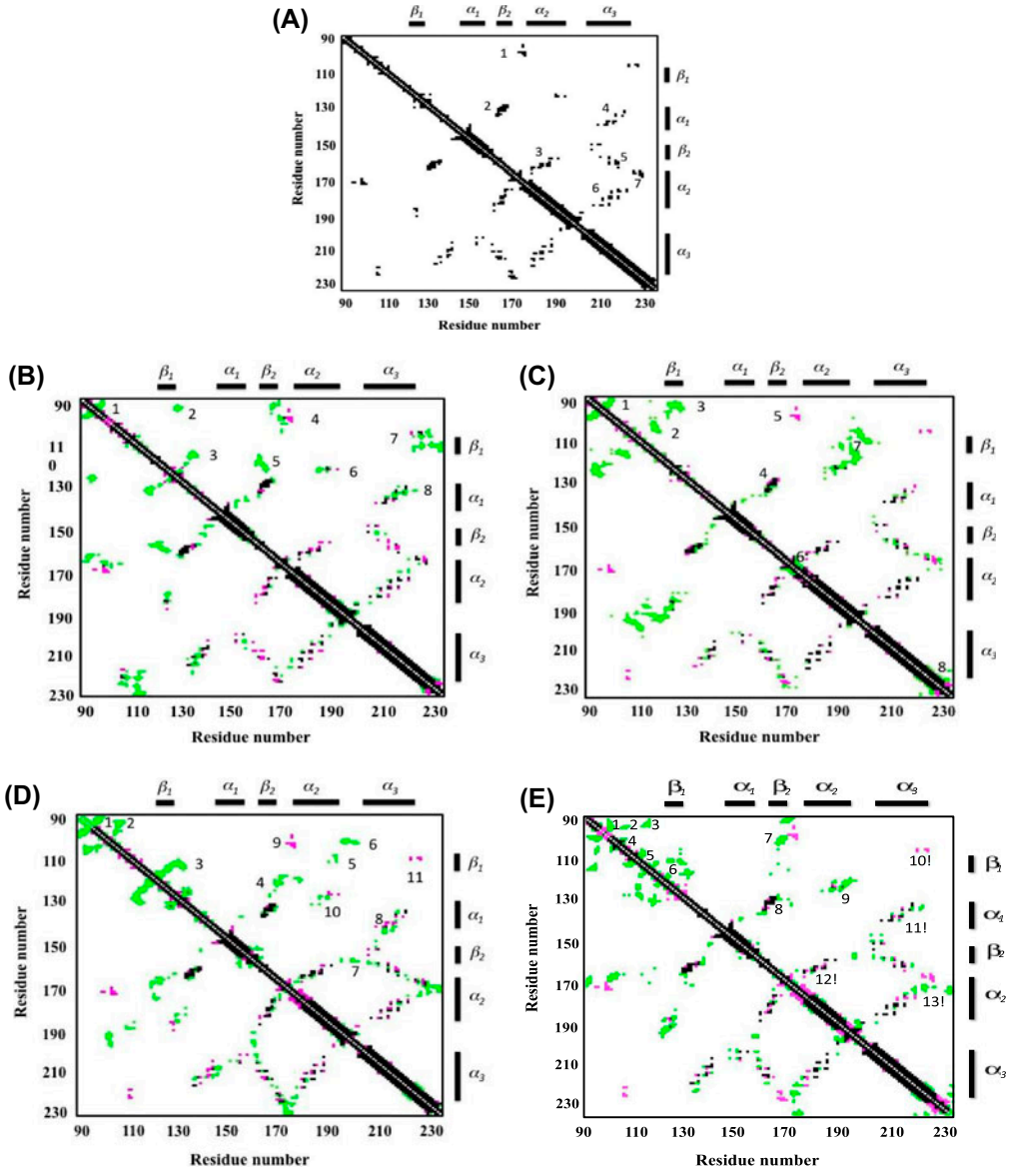

Figure 6. The Cα contact maps after the first round of simulations. (A) Original WT monomer. (B) WT monomer after simulation superimposed on original WT monomer's contact map. (C) E219K monomer after simulation superimposed on original WT monomer's contact map. (D) V210I monomer after simulation superimposed on original WT monomer's contact map. (E) Q212P monomer after simulation superimposed on original WT monomer's contact map. Green dots showing newly formed contacts, pink show disappeared contacts, and black dots show common contacts between structure models after 30-ns simulation and native WT structure.

115–118 (region 2). Besides, a considerably large contact region (region 8) is formed between residues 105–125 of N-terminal tail and residues 185–200 including α_2 and turn 2; thus, in the original WT structure the N-terminal tail sinks closer to the C-terminal of α_3, while it makes contacts to the residues in the opposite side of the protein closer to α_2 and C-terminal of α_3. In addition, the helix elongation within residues 221–227 (region 12) is notable. In total, the main effects of E219K mutation on HuPrP structure, includes extensive contacts between the N-terminal tail residues (regions 1–3), N-terminal tail and α_2 (region 8), elongation of β_1 and β_2 strands (contacts at region 4), and elongation of α_2 helix (region 6).

3.4. *E219K stabilizes interactions of hydrophobic core*

Van Der Kamp and Daggett reported possibility of hydrophobic core exposure as a result of pathogenic mutations in hydrophobic core (Van der Kamp & Daggett, 2010). In the present study, close contacts of aromatic and hydrophobic interactions between residues located at the interface of the β_2-α_2 loop and the

C-terminus of the α_3 helix were measured to examine reported results by Van Der Kamp and Daggett (Table 1). The considerably longer average distances between Met166 and Tyr218 in monomeric forms of models are observed in mutations in hydrophobic core with respect to WT protein before and after 30-ns simulations (Table 2). Disruption of interactions between the β_2-α_2 loop and the α_3 helix in the mutations at the hydrophobic

Table 2. The average distances between residues at the interface of the β_2-α_2 loop and the α_3 helix in different mutations.

	Before simulation			After 30-ns simulation		
Mutant	M166(C_ε)–Y218 ($C_{\delta 2}$)	M166(C_ε)–Y225 ($C_{\varepsilon 1}$)	F175(C_ζ)–Y218 (C_β)	M166(C_ε)–Y218 ($C_{\delta 2}$)	M166(C_ε)–Y225 ($C\varepsilon_1$)	F175(C_ζ)–Y218 (C_β)
E219K	4.1 ± 0.2*	4.0 ± 0.1*	3.9 ± 0.1*	9.0	6.9	4.3
WT	3.7 ± 0.1*	5.4 ± 0.0*	4.0 ± 0.0*	4.4	6.9	4.2
Q212P	9.8 ± 1.8*	14.9 ± 2.7*	4.7 ± 0.4*	9.2	10.5	9.6
V210I	9.6 ± 0.3*	4.4 ± 0.8*	6.9 ± 0.5*	5.6	10	10.7

*Data adapted from Biljan et al. (2012).

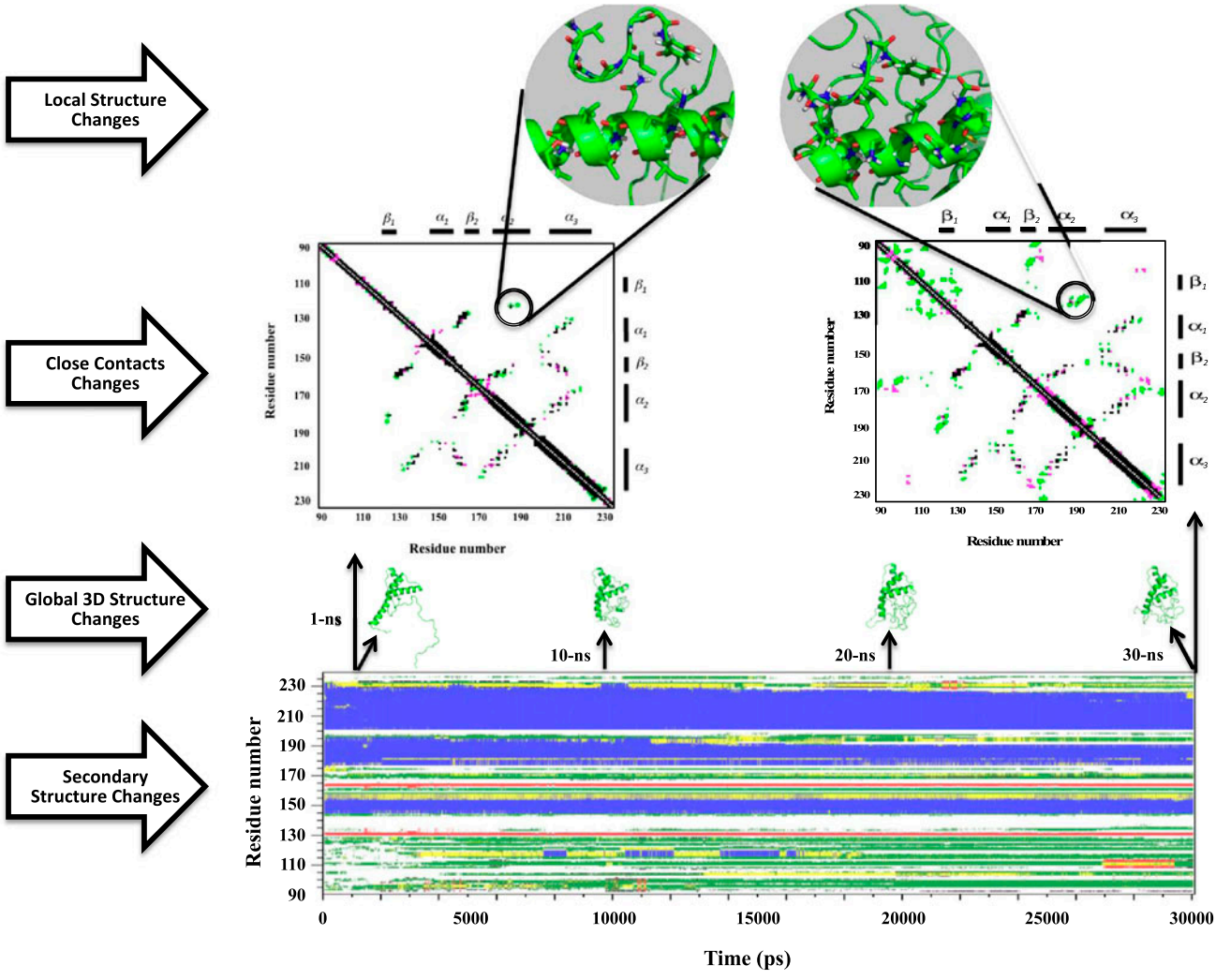

Figure 7. Summary of our methodology for analysis of the obtained results during 30-ns MD simulations (the case of Q212P in monomeric form during the first round of simulation is presented in this figure). Secondary structure changes, global 3D structure changes, close contact changes, and local structure changes, were analyzed during 30-ns MD simulations in different levels. This figure shows the process of new close contact formation between residues 119–126 and α2 residues form after 30-ns MD simulation.

core is further manifested by increased Met166–Tyr225 and Phe175–Tyr218 inter-residue average distances, before and after 30-ns simulations, in the Q212P and V210I mutants compared to E219K, and in the WT models (Table 2). In the case of E219K, except longer average distances between Met166 and Tyr218 in monomeric form after 30-ns simulations, the contacts between the β_2-α_2 loop and the α_3 helix are almost similar or even diminished with respect to WT model. However, average distances between Met166 and Tyr218 in E219K-WT dimeric form after 30-ns are decreased to 3.9 angstrom, which is less than the similar distances in WT protein. Other findings also have been reported about the other disease-related mutations of HuPrP (Lee et al., 2009; Meli, Gasset, & Colombo, 2009; Rossetti, Cong, Caliandro, Legname, & Carloni, 2011; Zhang, Swietnicki, Zagorski, Surewicz, & Sönnichsen, 2000).

4. Conclusion

Molecular dynamics simulation is a useful tool to study the effect of pathogenic mutations in prion proteins (Van der Kamp & Daggett, 2011). Recently, many MD simulation studies have been done on pathogenic mutations in prion proteins such as G131V, S132I, A133V, H140R, D178V, D178N, V180I, T183A, H187R, F198V, F198S, E200K, V203I, R208C, V210I, Q212P mutations, etc. (Behmard, Abdolmaleki, Asadabadi, & Jahandideh, 2011; Chebaro & Derreumaux, 2009; De Simone, Dodson, Verma, Zagari, & Fraternali, 2005; Guo et al., 2012; Hosszu et al., 2010; Jahandideh & Zhi, 2014; Levy & Becker, 2002; Rossetti, Giachin, Legname, & Carloni, 2010; Van der Kamp & Daggett, 2010; Zhang, Dai, Iwamoto, & Ouyang, 2006). Generally, pathogenic mutations decrease the stability of prion protein, but few of them have obvious influence on the secondary structures, which causes the elongation of β-sheet. Previous studies clearly show that different mutants undergo different misfolding pathways and have different pathogenesis.

By performing all-atom MD simulations, the atomic-level structural variations for protective mutation, and the disease-related mutations in monomeric and dimeric forms were studied to understand the structural and dynamic changes related to misfolding and protectivity effect. Figure 7 shows our methodology for the analysis of MD results during 30-ns simulation in different levels, from secondary structure changes to targeted local structure changes by changes in close contact patterns. Briefly, after 30-ns simulation we analyzed secondary structure changes during simulation time; then, close contact maps were generated and changes in contacts map during simulation time were inspected. Finally, we focused on local structures of changed close contacts.

After 30-ns simulations of both monomeric and dimeric forms, we observe a fair similarity between the WT and the mutants' overall 3D structure of core regions. However, clear differences are obvious between protective and disease-related mutations. These differences include the changes in the secondary structures, such as the formation of beta-sheets in the disease related mutations and helix elongation in protective mutation, the changes of local close contacts, the observed solvent exposure of hydrophobic core in the disease-related mutations, and significant increases in overall flexibility of protective mutation during 30-ns simulation.

Our results offer some evidence, supporting the *dominant-negative effect* of protective mutation, reported in previous investigations (Hizume et al., 2009; Perrier et al., 2002). Furthermore, our data suggests that individuals heterozygous for lysine at codon 219 are protected against sCJD because the HuPrPs derived from two allelic variants interfere with each other in the conversion process due to their incompatible structures and dynamics.

References

Behmard, E., Abdolmaleki, P., Asadabadi, E. B., & Jahandideh, S. (2011). Prevalent mutations of human prion protein: A molecular modeling and molecular dynamics study. *Journal of Biomolecule Structure & Dynamics, 29*, 379–389.

Biljan, I., Giachi, G., Ilc, G., Zhukov, I., Plavec, J., & Legname, G. (2012). Structural basis for the protective effect of the human prion protein carrying the dominant-negative E219K polymorphism. *Biochemical Journal, 446*, 243–251.

Chebaro, Y., & Derreumaux, P. (2009). The conversion of helix H2 to b-sheet is accelerated in the monomer and dimer of the prion protein upon T183A mutation. *Journal of Physical Chemistry B, 113*, 6942–6948.

Chen, W., Van der Kamp, M. W., & Daggett, V. (2010). Diverse effects on the native β-sheet of the human prion protein due to disease-associated mutations. *Biochemistry, 49*, 9874–9881.

Crozet, C., Lin, Y. L., Mettling, C., Mourton-Gilles, C., Corbeau, P., Lehmann, S., & Perrier, V. (2004). Inhibition of PrP^{Sc} formation by lentiviral gene transfer of PrP containing dominant negative mutations. *Journal of Cell Science, 117*, 5591–5597.

De Simone, A., Dodson, G. G., Verma, C. S., Zagari, A., & Fraternali, F. (2005). Prion and water: Tight and dynamical hydration sites have a key role in structural stability. *Proceedings of the National Academy of Sciences USA, 102*, 7535–7540.

DeLano, W. L. (2002). *The PyMOL molecular graphics system*. Palo Alto, CA: DeLano Scientific.

Geoghegan, J. C., Miller, M. B., Kwak, A. H., Harris, B. T., & Supattapone, S. (2009). Trans-dominant inhibition of prion propagation *in vitro* is not mediated by an accessory cofactor. *PLOS Pathology, 5*(7), e1000535.

Guo, J., Ren, H., Ning, L., Liu, H., & Yao, X. (2012). Exploring structural and thermodynamic stabilities of human prion protein pathogenic mutants D202N, E211Q and Q217R. *Journal of Structural Biology, 178*, 225–232.

Hizume, M., Kobayashi, A., Teruya, K., Ohashi, H., Ironside, J. W., Mohri, S., & Kitamoto, T. (2009). Human prion protein (PrP) 219K is converted to PrP^{Sc} but shows heterozygous inhibition in variant Creutzfeldt–Jakob disease infection. *Journal of Biological Chemistry, 284*, 3603–3609.

Hosszu, L. L., Tattum, M. H., Jones, S., Trevitt, C. R., Wells, M. A., Waltho, J. P., … Clarke, A. R. (2010). The H187R mutation of the human prion protein induces conversion of recombinant prion protein to the PrP^{Sc}-like form. *Biochemistry, 49*, 8729–8738.

Jahandideh, S., & Zhi, D. (2014). Systematic investigation of predicted effect of nonsynonymous SNPs in human prion protein gene: A molecular modeling and molecular dynamics study. *Journal of Biomolecule Structure & Dynamics, 32*, 289–300.

Kaneko, K., Zulianello, L., Scott, M., Cooper, C. M., Wallace, A. C., James, T. L., … Prusiner, S. B. (1997). Evidence for protein X binding to a discontinuous epitope on the cellular prion protein during scrapie prion propagation. *Proceedings of the National Academy of Sciences USA, 94*, 10069–10074.

Knaus, K. J., Morillas, M., Swietnicki, W., Malone, M., Surewicz, W. K., & Yee, V. C. (2001). Crystal structure of the human prion protein reveals a mechanism for oligomerization. *Nature Structural Biology, 8*, 770–774.

Lee, C. I., Yang, Q., Perrier, V., & Baskakov, I. V. (2007). The dominant-negative effect of the Q218K variant of the prion protein does not require protein X. *Protein Science, 16*, 2166–2173.

Lee, S., Antony, L., Hartmann, R., Knaus, K. J., Surewicz, K., Surewicz, W. K., & Yee, V. C. (2009). Conformational diversity in prion protein variants influences intermolecular β-sheet formation. *EMBO Journal, 29*, 251–262.

Levy, Y., & Becker, O. M. (2002). Conformational polymorphism of wild-type and mutant prion proteins: Energy landscape analysis. *Proteins: Structure Function, & Bioinformatics, 47*, 458–468.

Liemann, S., & Glockshuber, R. (1998). Transmissible spongiform encephalopathies. *Biochemical and Biophysical Research Communications, 250*, 187–193.

Lukic, A., Beck, J., Joiner, S., Fearnley, J., Sturman, S., Brandner, S., … Mead, S. (2010). Heterozygosity at polymorphic codon 219 in variant Creutzfeldt–Jakob disease. *Archives of Neurology, 67*, 1021–1023.

Meli, M., Gasset, M., & Colombo, G. (2009). Dynamic diagnosis of familial prion diseases supports the β_2-α_2 loop as a universal interference target. *PLOS ONE, 6*, e19093.

Pan, K. M., Baldwin, M., Nguyen, J., Gasset, M., Serban, A., Groth, D., … Chohen, F. E. (1993). Conversion of alpha-helices into beta-sheets features in the formation of the scrapie prion proteins. *Proceedings of the National Academy of Sciences USA, 90*, 10962–10966.

Panegyres, P. K., Toufexis, K., Kakulas, B. A., Cernevakova, L., Brown, P., Ghetti, B., … Dlouhy, S. R. (2001). A new PRNP mutation (G131V) associated with Gerstmann–Sträussler–Scheinker disease. *Archives of Neurology, 58*, 1899–1902.

Perrier, V., Kaneko, K., Safar, J., Vergara, J., Tremblay, P., DeArmond, S. J., … Wallace, A. C. (2002). Dominant-negative inhibition of prion replication in transgenic mice. *Proceedings of the National Academy of Sciences USA, 99*, 13079–13084.

Polymenidou, M., Prokop, S., Jung, H. H., Hewer, E., Peretz, D., Moos, R., … Aguzzi, A. (2011). Atypical prion protein conformation in familial prion disease with PRNP P105T mutation. *Brain Pathology, 21*, 209–214.

Prusiner, S. B. (1982). Novel protein acetous infectious particles cause scrapie. *Science, 216*, 136–144.

Rossetti, G., Cong, X., Caliandro, R., Legname, G., & Carloni, P. (2011). Common structural traits across pathogenic mutants of the human prion protein and their implications for familial prion diseases. *Journal of Molecular Biology, 411*, 700–712.

Rossetti, G., Giachin, G., Legname, G., & Carloni, P. (2010). Structural facets of disease- linked human prion protein mutants: A molecular dynamic study. *Proteins: Structure, Function, & Bioinformatics, 78*, 3270–3280.

Shibuya, S., Higuchi, J., Shin, R. W., Tateishi, J., & Kitamoto, T. (1998). Codon 219 Lys allele of PRNP is not found in sporadic Creutzfeldt–Jakob disease. *Annals of Neurology, 43*, 826–828.

Soldevila, M., Calafell, F., Andres, A. M., Yague, J., Helgason, A., Stefansson, K., & Bertranpetit, J. (2003). Prion susceptibility and protective alleles exhibit marked geographic differences. *Human Mutation, 22*, 104–105.

Surewicz, W. K., & Apostol, M. I. (2011). Prion protein and its conformational conversion: A structural perspective. *Topics in Current Chemistry, 305*, 135–167.

Van der Kamp, M. W., & Daggett, V. (2010). Pathogenic mutations in the hydrophobic core of the human prion protein can promote structural instability and misfolding. *Journal of Molecular Biology, 404*, 732–748.

Van der Kamp, M. W., & Daggett, V. (2011). Molecular dynamics as an approach to study prion protein misfolding and the effect of pathogenic mutations. *Topics in Current Chemistry, 305*, 169–197.

Van Der Spoel, D., Lindahl, E., Hess, B., Groenhof, G., Mark, A. E., & Berendsen, H. J. (2005). GROMACS: Fast, flexible, and free. *Journal of Computational Chemistry, 26*, 1701–1718.

Vehlow, C., Stehr, H., Winkelmann, M., Duarte, J. M., Petzold, L., Dinse, J., & Lappe, M. (2011). CMView: Interactive contact map visualization and analysis. *Bioinformatics, 27*, 1573–1574.

Zahn, R., Liu, A., Luhrs, T., Riek, R., von Schroetter, C., Lopez Garcia, F., … Wuthrich, K. (2000). NMR solution structure of the human prion protein. *Proceedings of the National Academy of Sciences USA, 97*, 145–150.

Zhang, Y., Dai, L., Iwamoto, M., & Ou-Yang, Z. (2006). Molecular dynamics study on the conformational transition of prion induced by the point mutation: F198S. *Thin Solid Films, 499*, 224–228.

Zhang, Y. B., Swietnicki, W., Zagorski, M. G., Surewicz, W. K., & Sönnichsen, F. D. (2000). Solution structure of the E200K variant of human prion protein: Implications for the mechanism of pathogenesis in familial prion diseases. *Journal of Biological Chemistry, 275*, 33650–33654.